



OPEN

Simple and versatile imaging of genomic loci in live mammalian cells and early pre-implantation embryos using CAS-LiveFISH

Yongtao Geng & Alexandros Pertsinidis✉

Visualizing the 4D genome in live cells is essential for understanding its regulation. Programmable DNA-binding probes, such as fluorescent clustered regularly interspaced short palindromic repeats (CRISPR) and transcription activator-like effector (TALE) proteins have recently emerged as powerful tools for imaging specific genomic loci in live cells. However, many such systems rely on genetically-encoded components, often requiring multiple constructs that each must be separately optimized, thus limiting their use. Here we develop efficient and versatile systems, based on *in vitro* transcribed single-guide-RNAs (sgRNAs) and fluorescently-tagged recombinant, catalytically-inactivated Cas9 (dCas9) proteins. Controlled cell delivery of pre-assembled dCas9-sgRNA ribonucleoprotein (RNP) complexes enables robust genomic imaging in live cells and in early mouse embryos. We further demonstrate multiplex tagging of up to 3 genes, tracking detailed movements of chromatin segments and imaging spatial relationships between a distal enhancer and a target gene, with nanometer resolution in live cells. This simple and effective approach should facilitate visualizing chromatin dynamics and nuclear architecture in various living systems.

The dynamic genome organization in the nucleus directs many important processes, such as gene expression regulation, epigenetic inheritance, recombination, DNA replication and genome maintenance, in normal physiology and in disease. Fluorescence *in-situ* hybridization (FISH) methods have been widely used to detect specific DNA sequences, providing a wealth of information on 3D genome architecture. However FISH relies on chemical fixation, precluding tracking real-time dynamics in live cells. Moreover, harsh treatments with high heat and denaturants might compromise the integrity of genomic structures, especially on the kilobase and nanometer scales. To address some of these limitations, fluorescent programmable DNA binding proteins have emerged as a promising tool for visualizing specific genomic loci in live cells. Fluorescent TALE proteins, engineered to recognize specific DNA sequences, such as major satellite and telomere repeats, were used to visualize repetitive DNA sequences in live human and mouse cells as well as in fly and mouse embryos^{1–3}. Although engineering a separate TALE protein is required for each genomic locus, the use of CRISPR-Cas9 proteins, whose DNA recognition can be programmed by a single-guide RNA, significantly simplified targeting^{4,5}. Multi-color approaches based on orthogonal dCas9 proteins^{6,7}, or by fusing various RNA protein binding motifs to the gRNA^{8–10}, have also been demonstrated.

Most of the previous CRISPR imaging applications focused on visualizing repetitive DNA elements, where the signal amplification from multiple bound dCas9 molecules facilitates detection. Although significantly more challenging, dCas9 can also be used to tag non-repetitive DNA elements, when programmed with multiple gRNAs that target a specific locus in tandem^{4,11,12}. However, robust tagging for non-repetitive locus imaging can be challenged by low efficiencies. Often the system needs to be engineered to optimize expression levels of fluorescent dCas9 as well as gRNAs. This issue is further exacerbated by the additional complexity of multi-color systems, which use multiple expression constructs, each one needing separate optimization, limiting the broad use of CRISPR for genome imaging applications.

Here we report a simple and versatile CRISPR imaging system based on *in vitro* transcribed gRNAs and fluorescent recombinant dCas9 proteins. Controlled cell delivery enables straightforward optimization of the system to achieve robust tagging and high signal-to-noise (SNR) imaging. Simultaneous delivery of multiple gRNAs is also simplified, allowing tandem tagging of endogenous loci. Using this approach, CRISPR/Cas9-mediated

Structural Biology Program, Memorial Sloan Kettering Cancer Center, New York, NY 10065, USA. ✉email: PertsinA@mskcc.org

in situ tagging of genomic loci in live cells, CAS-LiveFISH, we achieve simultaneous multi-color tagging of up to 3 genes and efficient tagging of low-repeat-containing and non-repetitive loci. We further show that pre-assembled RNPs can successfully visualize genomic loci in live pre-implantation mouse embryos, as a proof-of-principle for CAS-LiveFISH imaging in more complex living systems. Finally, we demonstrate tracking of sub-diffusive motions of chromatin loci and 2-color nanometer distance measurements between a distal enhancer and a target gene in live cells. These results illustrate the efficiency, versatility and capability of CAS-LiveFISH for imaging genome organization and dynamics.

Results

Imaging of genomic loci by delivery of in vitro transcribed gRNAs and recombinant fluorescent dCas9. We first test the ability of in vitro transcribed gRNAs to target cell-expressed dCas9-EGFP to specific genomic loci (Fig. 1a). We deliver gRNAs targeting telomeres in live U-2 OS cells using electroporation, together with a plasmid encoding for BFP-LifeAct to assist identification of transfected cells. Telomeres are visible in transfected cells, while a control gRNA (sgGal4) does not result in any nuclear puncta, demonstrating the specificity of the approach (Fig. 1b, Supplementary Fig. 1). As an alternative, in vitro transcribed gRNAs are microinjected in live U-2 OS cells, together with Alexa 647-Benzylguanine, as a nuclear “counter-stain” for SNAP-tagged RNA Pol II. Like electroporation, microinjection of gRNAs results in robust dCas9-EGFP nuclear puncta (Fig. 1c), suggesting efficient tagging of telomeres and illustrating versatility among cell delivery approaches.

Based on the results with in vitro transcribed gRNAs, we next test the ability of pre-assembled fluorescent dCas9-gRNA ribonucleoproteins (RNPs) to tag specific genomic loci (Fig. 1d). We first prepare fluorescent dCas9-SNAPf and dCas9-CLIPf proteins (Supplementary Fig. 2) and validate their in vitro DNA binding activity and specificity when assembled with in vitro transcribed gRNAs into RNPs (Supplementary Fig. 3). We next test the preassembled RNPs in live cells. Delivery of Alexa 647-labelled RNPs targeting telomeres into U-2 OS cells by microinjection results in numerous nuclear puncta (Fig. 1e), similar to that achieved by telomere tagging with cell-expressed dCas9-EGFP. Co-delivery of two types of RNPs into live U-2 OS cells, TMR-labelled RNPs targeting telomeres and Alexa 647-labeled RNPs targeting α -satellite repeats, results in distinct, non-overlapping nuclear puncta (Fig. 1f). To further test the specificity of tagging, we assemble Atto 488- or TMR-labelled RNPs targeting telomeres, and non-targeting (sgGal4) Alexa 647-labelled RNPs as a control. Co-delivery into live HeLa cells results in robust telomere tagging, visible in the Atto 488 or TMR channel, while no nuclear puncta are observable in the Alexa 647 channel (Fig. 1g). Together, these results are consistent with in vitro competition experiments that show minimum cross-talk (Supplementary Fig. 4a,b) and illustrate specificity in two-color genome tagging as well as versatility among cell types.

CAS-LiveFISH imaging of genomic loci in live pre-implantation embryos. Although numerous demonstrations of CRISPR-based genomic imaging have been reported in cultured cells, applications in living organisms have been thus far limited. We reason that the versatility of the pre-assembled fluorescent RNP system could also be used to tag genomic loci in live mammalian pre-implantation embryos. We thus microinject preassembled TMR-labelled dCas9 RNPs targeting telomeres, into 2-cell stage mouse embryos (Fig. 2a). Nuclear TMR puncta can be discerned (Fig. 2b), while a co-injected Alexa 647-Gal4 RNPs show only diffuse nuclear signal (Supplementary Fig. 5). TMR-tagged telomeres can be also observed at the 4-cell stage, ~1 day after microinjection (Fig. 2c), after the second cleavage division, indicating that fluorescent RNPs are stable enough in vivo to potentially track dynamics occurring over ~1 day time-scales in the early mouse embryo. These results show successful proof-of-principle use of the CAS-LiveFISH system for imaging genomic loci in live mammalian embryos.

Pools of pre-assembled RNPs enable visualizing the HPV-18 integration site in live HeLa cells. HeLa cells contain a genomic integration site of Human Papilloma Virus 18 (HPV-18) near the *MYC* oncogene (Fig. 3a). HPV integration plays a prominent role in the initiation of cervical cancers¹³ and in HeLa cells the HPV integration site creates a powerful transcriptional enhancer that drives *MYC* activation¹⁴. The HeLa HPV-18 integration site contains parts of the viral genome, as well as local integration-associated rearrangements of the host genome, with host and viral sequences amplified to copy numbers of ~4–30¹⁴.

We design 36 distinct gRNAs targeting the HPV integration site and assemble them with Alexa 647 dCas9 into fluorescent RNPs. Delivery of this HPV-targeting pool of RNPs into live HeLa cells typically results in ~2–4 nuclear puncta per cell (Fig. 3b,c). Occasionally we also resolve doublets in close proximity, suggestive of replicated loci in S/G2⁴. To verify the specificity of dCas9 tagging, we perform FISH with a probe labelling the extended *MYC* locus. Two-color imaging shows that the HPV-Alexa 647 puncta are within ~200–300 nm from the centroid of the *MYC* FISH puncta (Supplementary Fig. 6a,b). These results demonstrate successful locus-specific tagging of the low-repeat containing HPV integration site, using pools of pre-assembled RNPs.

Multiplex CAS-LiveFISH imaging of up to 3 genes. We reason that the minimal crosstalk between separately assembled two-color RNPs should also be extendable to higher multiplexing. We thus assemble Atto 488- and TMR-labeled dCas9 RNPs programmed with gRNAs targeting the *MUC1* and *MUC4* genes, respectively, and co-deliver them together with Alexa 647-HPV RNPs in live HeLa cells (Supplementary Fig. 7). 3-color imaging reveals robust and distinct puncta for Atto 488, TMR and Alexa 647, indicating efficient and specific simultaneous tagging of 3 separate genes. Higher multiplexing should also be achievable by adding more spectral channels and/or by spectral unmixing techniques.

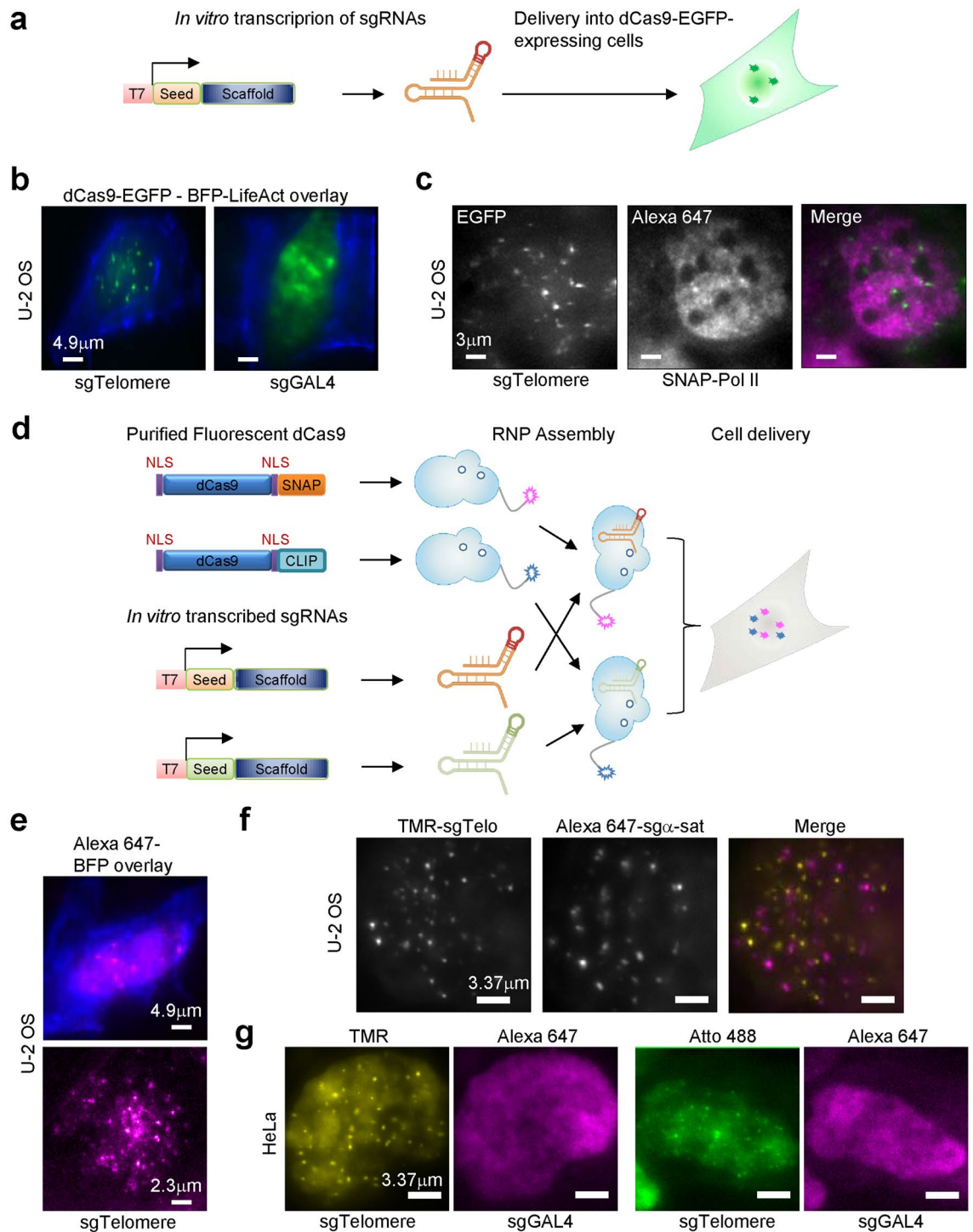


Figure 1. Imaging genomic loci in live cells with CAS-LiveFISH. **(a)** Schematic of cell delivery of *in vitro* transcribed gRNAs. **(b,c)** Visualization of telomeres in U-2 OS cells stably expressing dCas9-EGFP, by electroporation **(b)** or microinjection **(c)** of an *in vitro* transcribed gRNA (sgTelomere). A non-targeting control (sgGal4) shows no discernible nuclear puncta **(b)**, demonstrating locus-specific tagging. In **(b)**, cells are imaged 20 h after electroporation. Co-delivery of a BFP-LifeAct-expressing plasmid **(b)** or Alexa 647-Benzylguanine **(c)** results in simultaneous visualization of actin filaments and RNA Polymerase II (SNAP-Pol II), respectively. **(d)** Schematic of recombinant fluorescent dCas9:sgRNA RNP assembly and cell delivery. **(e–g)** Visualization of genomic loci in U-2 OS **(e)** and HeLa **(f,g)** cells using pre-assembled dCas9-gRNA RNPs. **(e)** Co-delivery of Alexa 647-RNPs targeting telomeres with a BFP-LifeAct plasmid. Bottom figure shows a cell a ~2–3 h after delivery, when BFP-LifeAct expression is not yet detected. Top panel shows a cell after ~0.5 days, when BFP-LifeAct expression is detected. **(f)** Co-delivery of TMR-RNPs targeting telomeres and Alexa 647-RNPs targeting a-satellite sequences shows distinct, non-overlapping nuclear puncta. **(g)** Co-injection of telomere-targeting Atto 488- or TMR-RNPs and non-targeting control Alexa 647-RNPs (sgGal4) shows no discernible nuclear puncta in the Alexa 647 channel, demonstrating locus-specific tagging and minimal cross-talk between colors.

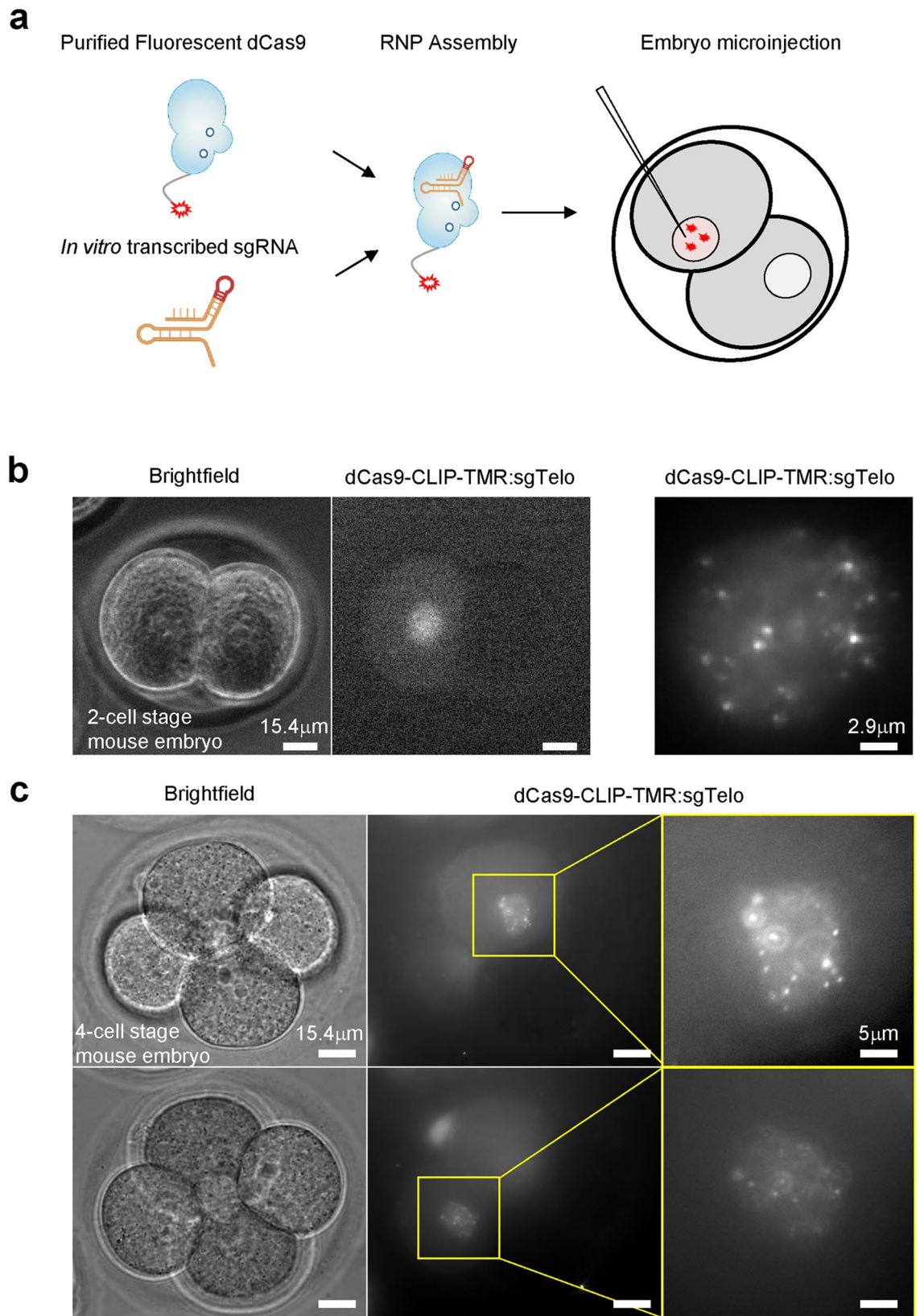


Figure 2. CAS-LiveFISH imaging in live mouse pre-implantation embryos. (a) Schematic of fluorescent RNP assembly and delivery into 2-cell stage embryos. (b) Left and middle panels: brightfield and fluorescence images of a live 2-cell stage embryo, with one cells microinjected with TMR-sgTelo RNPs. Images obtained with a Zeiss epi-fluorescence microscope. Right panel: maximum-intensity projection of a 20 μm z-stack of the injected cell nucleus, imaged with the home-made higher-sensitivity microscope setup. Bright nuclear puncta are visible, indicating robust telomere labelling. (c) Brightfield and fluorescence images of a 4-cell stage embryo, 1 day after injecting one of the cells at the 2-cell stage with TMR-sgTelo RNPs. Nuclear puncta are visible in the two daughter nuclei. Top and bottom images correspond to two different focal planes, to bring each of the two nuclei in focus.

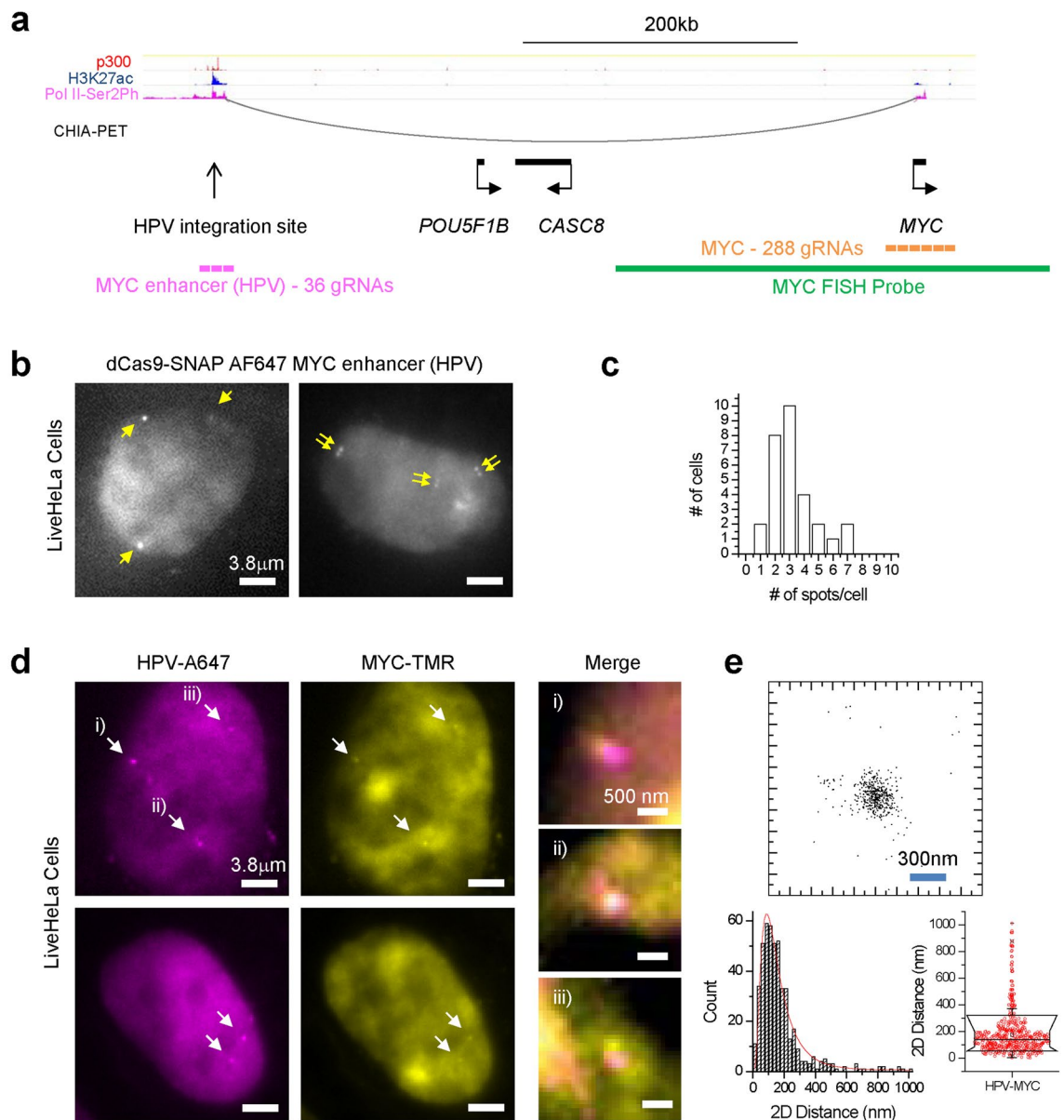


Figure 3. Pools of pre-assembled RNPs enable visualizing the *MYC* locus in live HeLa cells. **(a)** Organization of the extended *MYC* locus through proximity ligation (ChIA-PET) and ChIP-Seq assays. HeLa Pol II ChIA-PET data (GSM832461)⁴⁰, as well as ChIP-Seq data for p300 (GSM935500), H3K27ac (GSM733684) and Pol2-Ser2Ph (GSM935383), are visualized using the WashU Epigenome Browser⁴¹. **(b)** Visualization of the HPV integration site using Alexa 647-labeled dCas9 RNPs, assembled with a pool of 36 distinct gRNAs. The right cell contains doublets of closely-spaced puncta, indicative of replicated loci in S/G2. **(c)** Distribution of number of discernible Alexa 647-HPV spots per cell. **(d)** Simultaneous two-color imaging of HPV integration site (Alexa 647) and *MYC* (TMR) using co-delivery of preassembled RNPs in live HeLa cells. **(e)** 2D scatter plot of relative positions and statistics (histogram and box plot) of 2D distances between Alexa 647-HPV and TMR-*MYC* in live HeLa cells. 2D distance is 177 ± 155 nm (mean \pm S.D.; $n = 472$ measurements from > 30 loci).

CAS-LiveFISH enables imaging spatial relations between HPV integration site and *MYC* in live HeLa cells.

Proximity-ligation assays, such as Hi-C and ChIA-PET, suggested that activation of *MYC* in HeLa cells by the transcriptional enhancer created at the HPV integration site involves long-range genomic interactions (Fig. 3a). However, the physical distances between enhancer and target loci at *MYC* have not been measured in live cells. To leverage CAS-LiveFISH for imaging spatial relationships between two genomic loci, we first create a pool of 288 in vitro transcribed gRNAs targeting ~ 40 kb around the *MYC* gene and assemble them with TMR-labelled dCas9 into fluorescent RNPs. Co-delivery of TMR-*MYC* and Alexa 647-HPV RNPs in live HeLa cells results in Alexa 647 puncta that often co-localize with TMR puncta (Fig. 3d). As a control, co-delivery of TMR-Gal4 and Alexa 647-HPV RNPs results in Alexa 647 puncta but no discernible TMR puncta (Supplementary Fig. 8), further indicating specific tagging of the two genomic loci with minimal crosstalk.

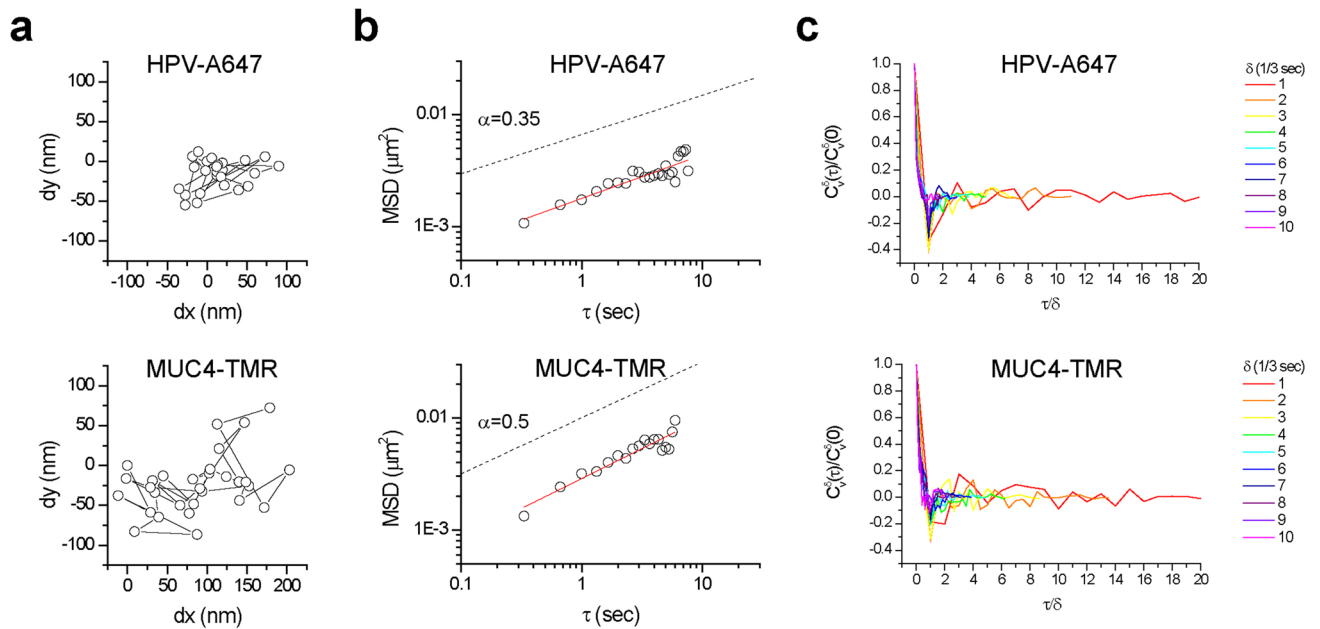


Figure 4. CAS-LiveFISH enables tracking the real-time motion of single gene loci. (a–c) Real-time tracking of Alexa 647-HPV (top) and TMR-MUC4 (bottom) motions. (a) Scatter plots showing the trajectory of single Alexa 647-HPV and TMR-MUC4 loci. (b) MSD vs. τ graphs show sub-diffusive motion, which is significantly stronger for HPV vs. *MUC4*. Red lines: linear fits, with $\alpha = 0.37 \pm 0.04$ and $\alpha = 0.53 \pm 0.05$ ($n = 31$ and 15 loci from multiple cells) for HPV and *MUC4* respectively. (c) Velocity autocorrelation functions, showing negative dips, indicative of movement inside a viscoelastic environment. HPV exhibits more pronounced negative dips than *MUC4*, indicating stronger confinement. The time axis is rescaled with the time delay parameter δ ; collapse of the curves indicates self-similar motions.

To measure the distances between TMR-MYC and Alexa 647-HPV we first perform a two-color nanometer registration procedure using fluorescent nanoparticles, which achieves a root-mean-square (r.m.s.) registration accuracy of 21 nm in x , 25 nm in y and 32 nm in 2D (Supplementary Fig. 9a–c). We further validate the precision of distance measurements in live cells using dual TMR-HPV and Alexa 647-HPV tagging. The two-color HPV-HPV distances have a tight distribution with an average 2D distance of ~ 60 nm, consistent with $\sigma_{xy} \sim 39$ nm 2D localization errors in each color ($\sigma_{x,y} \sim 27$ nm each in x, y) and 32 nm two-color 2D registration errors (Supplementary Fig. 10a,b). Using this two-color nanometer co-localization procedure, we measure the relative distances between TMR-MYC and Alexa 647-HPV nuclear puncta. We observe a range of 2D MYC-HPV distances, with the majority ($\sim 75\%$) being within 200 nm proximity, while a smaller sub-population ($\sim 10\%$) is further separated, at distances of 300 nm–1 μm (Fig. 3e). These results illustrate how two-color tagging of genomic loci can provide insights into spatial relations of *cis*-elements and target genes, with nanometer resolution in live cells.

Pre-assembled RNPs enable tracking the real-time motion of single gene loci. Understanding the movements of genomic loci in the nucleus is important for elucidating key processes such as gene regulation, DNA translocations and recombination. We use dCas9 RNP tagging and analyze the movement of the *MUC4* gene as well as the HPV integration site in live HeLa cells (Fig. 4a, Supplementary Video 1). The mean-squared-displacement (MSD) vs. time of both *MUC4* and HPV follow a scaling behaviour, $\text{MSD} \sim D t^\alpha$, with $\alpha < 1$ (Fig. 4b), indicating sub-diffusive motion, typical for tagged genomic loci. For *MUC4* $\alpha \approx 0.5$, in close agreement with previously observed $\alpha \approx 0.5$ for other endogenous genes and *cis*-elements^{11,15}. Scaling exponent $\alpha = 0.5$ characterizes the movement of individual monomers in a polymer chain (Rouse model)¹⁶. Interestingly, the motion of HPV appears strongly sub-diffusive, with $\alpha \approx 0.35$, significantly deviating from the free polymer-like physical picture. This confined motion could reflect spatial constraints such as local compartmentalization, highly cross-linked chromatin chains or other possible mechanisms^{16,17}. We also analyzed the velocity autocorrelation function (ACF) for the *MUC4* and HPV traces¹⁸. The velocity ACFs for both loci exhibit negative dips (Fig. 4c), indicating that the movement dynamics might be dominated by restoring forces often occurring inside a viscoelastic environment^{16,18,19}. Both loci exhibit self-similar motions, as the velocity ACFs collapse upon time-axis rescaling. The HPV velocity ACF exhibits a more pronounced negative dip than *MUC4*, consistent with the more strongly confined nature of the HPV motion vs. *MUC4*. Taken together, these results demonstrate how pre-assembled fluorescent RNP tagging can provide quantitative insights into the detailed movements of specific genomic loci in the nucleus of live cells.

Discussion

Here we demonstrate CAS-LiveFISH, an approach for visualizing specific genomic loci in live mammalian cells and early embryos. CAS-LiveFISH relies on cell delivery of pre-assembled fluorescent dCas9-gRNA RNPs, bypassing the need for extensive genetic manipulations and optimization of multiple expression constructs.

Previous works had begun to recognize the versatility of pre-assembled RNPs for genomic imaging. A variant of FISH (CAS-FISH), based on fluorescent dCas9 RNPs instead of DNA hybridization probes²⁰, showed rapid, cost-effective and convenient multi-color labelling of genomic loci, in fixed cells. More recently, use of dCas9 RNPs with fluorescent CRISPR RNAs (crRNAs) achieved high SNR detection of highly-repetitive genomic loci in cell lines, as well as in primary human cells²¹. The latter study also illustrated the potential of RNP-based approaches for medical diagnostics and for genomic imaging in systems that are not readily amenable to genetic manipulations. Here we significantly expand these previous works by demonstrating robust and efficient imaging of specific low-repeat containing and non-repetitive genomic loci, in live cells. dCas9 RNPs with fluorescent crRNAs could potentially achieve higher detection SNR, however use of fluorescent dCas9 and non-fluorescent in vitro transcribed gRNAs is significantly more cost-effective than pools of 10–100 s of individually chemically synthesized and purified fluorescent crRNAs. Future developments of low-cost methods to prepare in vitro transcribed pools of fluorescent gRNAs, such as using dye-binding aptamers^{22,23}, could enable increased detection SNR, due to the rapid degradation of background gRNAs that are not “protected” in a target DNA-bound dCas9:RNA:DNA ternary complex. Finally, combining our DNA targeting RNP system with RNA targeting CRISPR proteins, such as dCas13^{21,24}, would facilitate simultaneous imaging of *cis*-elements, target genes and nascent transcripts, as well as various other chromatin associated RNAs. Such direct visualization approaches would transform our ability to probe the links between genome organization and gene expression regulation as well as the nuclear organization, dynamics and function of non-coding regulatory RNAs.

CAS-LiveFISH by delivery of pre-assembled dCas9 RNPs can also be extended to imaging genomic loci in live early mouse embryos. The fluorescent RNPs are stable enough to potentially image over ~ 1 day-long time-scales. With emerging microscopy techniques to image in thick multi-cellular samples with increased sensitivity and resolution^{25–27}, imaging fainter signals, down to single non-repetitive genomic loci, and possibly together with simultaneous and coincidental single locus activity readouts and detection of regulatory molecules should also be within reach. These new capabilities could facilitate visualizing several important genomic processes at specific gene loci, in the context of early mammalian development.

A long-standing “mystery” of genome biology is how distal enhancers communicate with target genes to activate transcription²⁸. Mechanisms involving direct physical interactions, such as long-range chromatin looping, are thought to facilitate this process, but it has been very challenging to directly measure the spatial relationships between distal enhancers and target genes in live cells. Progress has been made by introducing artificial exogenous tags, such as arrays of target sites for bacterial DNA-binding proteins^{29,30}. CAS-LiveFISH enables directly tagging and imaging the endogenous genomic sequences, without needing genomic integrations of exogenous tags and possibly better reflecting the native chromatin organization. Our observations in live HeLa cells reveal that the distal enhancer created at the HPV integration site is often in < 200 nm proximity to the target *MYC* gene. An emerging view of distal gene regulation mechanisms proposes that approximate enhancer-promoter proximity^{28,30}, rather than direct molecular contact, might be adequate for transcription activation. High-local concentrations of Pol II regulatory factors (RFs) created around the enhancer might thus facilitate such action-at-a-distance. Interestingly, the physical distances are within the range (~ 200 nm) over which Pol II RFs cluster in the vicinity of pluripotency genes like *Pou5f1* (aka *Oct4*) and *Nanog* in embryonic stem cells¹⁵. CAS-LiveFISH, combined with molecular imaging of Pol II RFs could further elucidate the physical nature and underlying genome topologies behind these important regulatory macromolecular assemblies.

Finally, the observations of highly sub-diffusive motion of the HPV integration site in HeLa cells are particularly striking. Previous work had also showed strongly sub-diffusive motions for Tetracycline operator arrays integrated in immunoglobulin gene segments in B-lymphocytes¹⁷. It was further postulated that such highly constrained motion might reflect a network of cross-linked chromatin, close to the boundary of a sol-gel phase transition. Intriguingly, such a picture might also apply to highly-active clusters of transcriptional enhancers, bound by high densities of transcription factors and various co-activator proteins^{28,31}. The HPV-16 integration site in a related cervical neoplasia cell line colocalizes with a prominent nuclear focus that contains large amounts of Brd4, Mediator and H3K27 acetylated chromatin³². Further extensions to simultaneously visualize the HPV integration site in HeLa cells, together with RNA Polymerase II and various Pol II regulatory factors, as recently demonstrated for endogenous genes in mouse embryonic stem cells¹⁵, will be critical for testing various models for the physical organization of this important class of transcription regulatory units and their links to activation of important oncogenes like *MYC*.

Methods

Mammalian and bacteria cell culture. HeLa and U-2 OS cells were grown in MEM (Life Technologies) and McCoy's 5A Medium (ATCC) respectively, without phenol-red, and supplemented with 10% fetal bovine serum (FBS) 100U/mL penicillin/streptomycin, 1 mM Sodium Pyruvate, 1× Non-Essential Aminoacids solution (NEAA) and 2 mM L-alanyl-L-glutamine (GlutaMAX). All mammalian cells were grown in a 5% CO₂ atmosphere at 37 °C, in a humidified incubator. *Escherichia coli* were cultured in Luria-Bertani (LB) or 2×YT medium, in a 37 °C shaking incubator. Required antibiotics were added to the medium at the following concentrations: ampicillin: 100 µg/ml; chloramphenicol: 34 µg/ml; kanamycin: 50 µg/ml. Bacterial cell growth was monitored periodically by determining the optical density of culture aliquots at 600 nm using NanoDrop 2000 (Thermo Scientific).

Recombinant dCas9 expression and purification. The gene encoding a catalytically inactive *Streptococcus pyogenes* Cas9 (D10A/H840A) (dCas9) was cloned into a pD451-SR vector that contained a synthetic DNA fragment comprised of SNAPf or CLIPf tag, a Precision protease site and a His10 affinity tag (synthesized by DNA2.0). The dCas9 sequence also contains two copies of a Nuclear Localization Signal (NLS) sequence, to facilitate nuclear import. The *S. pyogenes* Cas9 D10A/H840A mutant was expressed in *E. coli* strain BL21 Rosetta 2 (DE3) (Novagen) and cultured in $2 \times$ YT medium at 18 °C for 16 h following induction with 0.2 mM IPTG. Cells were lysed in 20 mM Tris pH 8.0, 500 mM NaCl, 1 mM TCEP, supplemented with protease inhibitor cocktail (Roche). Clarified lysate was mixed with Ni-NTA agarose at 4 °C for 2 h (Qiagen). Bound protein was eluted in 20 mM Tris pH 8.0, 250 mM NaCl, 10% glycerol and 150 mM imidazole. The eluted protein were dialyzed overnight against 20 mM HEPES pH 7.5, 150 mM KCl, 1 mM TCEP, 10% glycerol and cleaved with PreScission protease to remove the His₁₀ affinity tag. The cleaved dCas9 protein was further purified with a 5 ml SP Sepharose HiTrap column (GE Life Sciences) in 20 mM HEPES pH 7.5, 150 mM KCl, 1 mM TCEP, 10% glycerol with a linear gradient of 150 mM–1 M KCl. Fractions containing dCas9 protein were pooled and the protein was concentrated with spin concentrators (Amicon Ultra 15, MWCO 10 k; Millipore), and after adding glycerol to 20% final concentration, flash-frozen in liquid nitrogen and stored at – 80 °C.

Fluorescent dCas9 labelling. For SNAP tag labelling, dCas9-SNAP protein samples were incubated with SNAP-Surface Alexa Fluor 647 (NEB S9136) at 37 °C for 30 min. For CLIP tag labelling, CLIP-Cell TMR star substrate or CLIP-Surface 488 substrate (NEB S9219 and S9232) was reacted with dCas9-CLIP proteins at 37 °C for 60 min. The excess fluorescent SNAP or CLIP substrate was removed with three washes using 10 K molecular weight (MWCO) spin concentrators (Millipore). Fluorescent dCas9 protein was stored in 20 mM HEPES pH 7.5, 150 mM KCl, 1 mM TCEP, 10% glycerol. Protein concentration and labelling efficiency were determined by measuring absorption spectra using a NanoDrop 2000 (Thermo Scientific). Calculated extinction coefficients at 280 nm are 141,670 and 140,180 for dCas9-SNAP and dCas9-CLIP respectively. Fluorescent dCas9 protein was flash-frozen in liquid nitrogen and stored at – 80 °C.

Preparation of In vitro transcribed gRNAs. A synthetic DNA fragment (IDT Gblocks) containing the full-length sequence of an optimized SP sgRNA⁴ was inserted into the BamHI and EcoRI sites of a modified pLVX-shRNA2 vector (Clontech) in which ZsGreen1 had been replaced by BFP. DNA templates for T7 transcription were prepared by PCR reactions using a common reverse primer and unique forward primers containing the T7 promoter and the seed sequence. The sgRNAs were in vitro synthesized with HiScribe T7 High Yield RNA Synthesis Kit (NEB). Transcription reactions were treated with RNase-free DNaseI (NEB) to digest the DNA template at 37 °C for 1 h. The sgRNAs were purified by phenol:chloroform: isoamyl alcohol (25:24:1) extraction and ethanol precipitation. The sgRNA pellets were dissolved in 20 mM HEPES (pH 7.5), 150 mM KCl, 10% glycerol and 1 mM TCEP. To refold purified sgRNAs, the sgRNAs were incubated at 70 °C for 5 min and slowly cooled down to room temperature. MgCl₂ was then added to 1 mM final concentration and the sgRNA samples were incubated at 50 °C for 5 min and slowly cooled down to room temperature. The sgRNAs concentration was estimated based on absorption measurements with a NanoDrop 2000 spectrophotometer (Thermo Scientific) and the samples were stored at – 80 °C. The sequences of nucleic acids used in this study can be found in Supplementary Tables 1–3.

Binding and electrophoretic mobility shift assays. Fluorescent dCas9-gRNA RNP complexes were assembled by incubating fluorescent dCas9 protein with a ~ 30-fold molar excess of sgRNA for 10 min at 37 °C. DNA binding reactions contained 5 nM Cy3- or Cy5-labelled DNA duplex and increasing concentrations of dCas9-sgRNA RNPs. In competition assays, unlabelled DNA duplex was added at 5 nM. DNA binding reactions were incubated for 15 min at 37 °C. dCas9-sgRNA:DNA tertiary complex formation was analyzed by 4% polyacrylamide native gel electrophoresis in 0.5× TBE buffer. Fluorescent bands in the gels were visualized using a fluorescent scanner (Typhoon; GE).

Mouse strains, husbandry and embryo recovery. Animal work was approved by MSKCC Institutional Animal Care and Use Committee (IACUC) and all methods were performed in accordance with the relevant IACUC guidelines and regulations. Animals were housed in a pathogen-free facility under a 12 h light/dark cycle. Mouse strain CD1 (Charles River) was used in this study. Embryos were obtained from mated females 6–12 weeks old. Embryo sex was not determined. To recover recently fertilized embryos, the infundibulum was flushed with FHM media (Sigma-Aldrich) and recovered embryos were washed and placed in FHM media for microinjection.

Delivery of sgRNAs and dCas9-gRNA RNPs into live cells and embryos. U-2 OS cells stably expressing spdCas9-GFP were nucleofected with Amaxa Cell Line Nucleofector Kit V (Lonza). Cells were detached with 0.05% trypsin/EDTA and spun down by centrifugation at 1000 rpm for 5 min. 1×10^6 cells were resuspended in 100 µl room-temperature Nucleofector Solution and mixed with sgRNA and a LifeAct-BFP expressing plasmid. Each sample was transferred into a cuvette and nucleofected using Nucleofector Program X-001. 500 µl of pre-equilibrated culture medium was then added to the cuvette and the cells were gently transferred into an 8-chamber coverglass (LabTek, 155411). Cells were imaged 4–6 h and 24 h after nucleofection.

To deliver fluorescent dCas9-gRNA RNP complexes into live cells, HeLa and U-2 OS cells were plated on 35 mm cover-glass bottom dishes (MatTek) and microinjected with fluorescent dCas9-sgRNA RNP complexes. The fluorescent dCas9 RNP complexes were reconstituted by combining fluorescent dCas9 protein with sgRNA

at a molar ratio of 1:30 ~ 1:50 in 20 mM HEPES (pH 7.5), 150 mM KCl, 10% glycerol and 1 mM TCEP at 37 °C for 10 min. Assembled RNP complexes were further diluted in microinjection buffer to about 100 nM–1 µM final concentration and filtered by spinning down at 2000 rpm for 2 min using a 0.22 µm sterilized centrifuge filter (COSTAR). The fluorescent dCas9-gRNA RNP complexes were loaded into glass microinjection capillary tips (Femtotips; Eppendorf) using a microloader pipette tip (Eppendorf) and injected into the nucleus of HeLa or U-2 OS cells using an Eppendorf FemtoJet Microinjector (Eppendorf). After media were changed, the cells were left to recover in the 37 °C/5% CO₂ incubator for ~ 3–5 h before imaging. For imaging genomic loci in mouse embryos, 2-cell stage mouse embryos were placed in FHM media under mineral oil in a round-bottom glass slide. After microinjection of fluorescent dCas9-gRNA RNPs, embryos were transferred to a 35 mm cover-glass bottom dish, into drops of KSOM media under mineral oil, and placed in a 37 °C/5% CO₂ incubator until imaging.

Live-cell and live-embryo imaging. Imaging was performed with a home-built microscope setup¹⁵, featuring a 60× 1.49 NA objective lens (Nikon MRD01691), 405 nm (Thorlabs diode), 488 nm (Coherent Sapphire HP 500 mW), 532 nm (Coherent Verdi G2 2000 mW) and 640 nm (Coherent Cube 100 mW) excitation lasers in epifluorescence configuration, a piezoelectric 3D nanopositioning stage (Physik Instrumente P-517.3CD and E-710.3CD controller) a quad-view 4-color imaging device (Photometrics) and an EM-CCD camera (Ixon3 897; Andor). Final magnification is 160 nm/pxl. Simultaneous two- or three-color imaging was performed on separate quadrants of the EM-CCD using the quad-view device. The quad-view was equipped with dichroics beam splitters (T495LPXRU, T560LPXR, and T645LPXR; Chroma) and emission filters (ET450/50 m, ET525/50 m, ET605/52 m, and ET700/50 m; Chroma) for separating and imaging the different colours. Imaging was performed at 3 frames/sec. Fine focusing was achieved by translating the sample in *z* with a nanopositioning stage (P-517.3CD, with E-710.3CD controller; Physik Instrumente). A home-built stage incubator and a separate objective lens heater maintained the sample at 37 °C. The stage incubator atmosphere was adjusted with independent O₂, N₂ and CO₂ mass-flow controllers (Omega). For some of the embryo imaging experiments, to achieve a larger field-of-view fitting whole embryos, we used a second epifluorescence microscope (Zeiss, Axiovert 200), equipped with an oil-immersion objective lens (Zeiss, Plan-apochromat 63× 1.4 NA), a mercury lamp illuminator (VSG HBO100/001-26E), filter sets for DAPI (used for BFP), GFP, TMR (used for RFP) and Cy5 (used for SiR), and a scientific CCD (Hamamatsu, ORCA Flash part #C47428012AG).

Image and data analysis, and two-color nanometer distance measurements. Image analysis was performed in IDL (ITT Visual Information Solution, version 8.0.1). First, nuclear puncta were identified using as local maxima in band-pass filtered and background-subtracted images³³. Then, we performed nanometer localization analysis for each identified punctum: to obtain *xy* coordinates for the image center of mass, with precision higher than the optical resolution, the processed images were fitted to a 2D elliptical Gaussian peak function using non-linear least-squares fitting^{34,35}. For calibrating the registration between *xy* coordinates in the Alexa 647 and TMR images with nanometer accuracy^{35,36}, we used the coordinates of 100 nm Tetraspek beads (ThermoFisher, T7284) scattered throughout the field of view. Two-color registration was performed using a second-order polynomial spatial warping transformation^{37,38}. MSD and velocity ACFs were calculated with a MATLAB routine (Matworks, version 2010b). Observed MSDs were corrected by subtracting a constant, MSD^{loc_error}, to account for the effect of localization errors³⁹. MSD^{loc_error} was estimated by tracking the relative motion of a single genomic locus, simultaneously tagged with dCas9-Alexa 647 and dCas9-TMR¹⁷. Graphing, linear least-squares fitting and statistical analysis was performed using Origin (OriginLab, version 8.5.0).

Received: 22 March 2021; Accepted: 1 June 2021

Published online: 09 June 2021

References

- Miyazari, Y., Ziegler-Birling, C. & Torres-Padilla, M. E. Live visualization of chromatin dynamics with fluorescent TALEs. *Nat. Struct. Mol. Biol.* **20**, 1321–1324 (2013).
- Ma, H., Reyes-Gutierrez, P. & Pederson, T. Visualization of repetitive DNA sequences in human chromosomes with transcription activator-like effectors. *Proc. Natl. Acad. Sci. USA* **110**, 21048–21053 (2013).
- Yuan, K., Shermoen, A. W. & O'Farrell, P. H. Illuminating DNA replication during *Drosophila* development using TALE-lights. *Curr. Biol.* **24**, R144–145 (2014).
- Chen, B. *et al.* Dynamic imaging of genomic loci in living human cells by an optimized CRISPR/Cas system. *Cell* **155**, 1479–1491 (2013).
- Anton, T., Bultmann, S., Leonhardt, H. & Markaki, Y. Visualization of specific DNA sequences in living mouse embryonic stem cells with a programmable fluorescent CRISPR/Cas system. *Nucleus* **5**, 163–172 (2014).
- Ma, H. *et al.* Multicolor CRISPR labeling of chromosomal loci in human cells. *Proc. Natl. Acad. Sci. USA* **112**, 3002–3007 (2015).
- Chen, B. *et al.* Expanding the CRISPR imaging toolset with *Staphylococcus aureus* Cas9 for simultaneous imaging of multiple genomic loci. *Nucleic Acids Res.* **44**, e75 (2016).
- Ma, H. *et al.* Multiplexed labeling of genomic loci with dCas9 and engineered sgRNAs using CRISPRainbow. *Nat. Biotechnol.* **34**, 528–530 (2016).
- Qin, P. *et al.* Live cell imaging of low- and non-repetitive chromosome loci using CRISPR-Cas9. *Nat. Commun.* **8**, 14725 (2017).
- Fu, Y. *et al.* CRISPR-dCas9 and sgRNA scaffolds enable dual-colour live imaging of satellite sequences and repeat-enriched individual loci. *Nat. Commun.* **7**, 11707 (2016).
- Gu, B. *et al.* Transcription-coupled changes in nuclear mobility of mammalian cis-regulatory elements. *Science* **359**, 1050–1055 (2018).
- Maass, P. G. *et al.* Spatiotemporal allele organization by allele-specific CRISPR live-cell imaging (SNP-CLING). *Nat. Struct. Mol. Biol.* **25**, 176–184 (2018).

13. Bosch, F. X., Lorincz, A., Munoz, N., Meijer, C. J. & Shah, K. V. The causal relation between human papillomavirus and cervical cancer. *J. Clin. Pathol.* **55**, 244–265 (2002).
14. Adey, A. *et al.* The haplotype-resolved genome and epigenome of the aneuploid HeLa cancer cell line. *Nature* **500**, 207–211 (2013).
15. Li, J. *et al.* Single-molecule nanoscopy elucidates RNA polymerase II transcription at single genes in live cells. *Cell* **178**, 491–506. e428 (2019).
16. Zhang, Y. & Dudko, O. K. First-passage processes in the genome. *Annu. Rev. Biophys.* **45**, 117–134 (2016).
17. Khanna, N., Zhang, Y., Lucas, J. S., Dudko, O. K. & Murre, C. Chromosome dynamics near the sol-gel phase transition dictate the timing of remote genomic interactions. *Nat. Commun.* **10**, 2771 (2019).
18. Weber, S. C., Spakowitz, A. J. & Theriot, J. A. Bacterial chromosomal loci move subdiffusively through a viscoelastic cytoplasm. *Phys. Rev. Lett.* **104**, 238102 (2010).
19. Lucas, J. S., Zhang, Y., Dudko, O. K. & Murre, C. 3D trajectories adopted by coding and regulatory DNA elements: First-passage times for genomic interactions. *Cell* **158**, 339–352 (2014).
20. Deng, W., Shi, X., Tjian, R., Lionnet, T. & Singer, R. H. CASFISH: CRISPR/Cas9-mediated in situ labeling of genomic loci in fixed cells. *Proc. Natl. Acad. Sci. USA* **112**, 11870–11875 (2015).
21. Wang, H. *et al.* CRISPR-mediated live imaging of genome editing and transcription. *Science* **365**, 1301–1305 (2019).
22. Autour, A. *et al.* Fluorogenic RNA Mango aptamers for imaging small non-coding RNAs in mammalian cells. *Nat. Commun.* **9**, 656 (2018).
23. Filonov, G. S., Moon, J. D., Svensen, N. & Jaffrey, S. R. Broccoli: Rapid selection of an RNA mimic of green fluorescent protein by fluorescence-based selection and directed evolution. *J. Am. Chem. Soc.* **136**, 16299–16308 (2014).
24. Yang, L. Z. *et al.* Dynamic imaging of RNA in living cells by CRISPR-Cas13 systems. *Mol. Cell* **76**, 981–997. e987 (2019).
25. Liu, T. L. *et al.* Observing the cell in its native state: Imaging subcellular dynamics in multicellular organisms. *Science*, **360**, eaaq1392 (2018).
26. McDole, K. *et al.* In toto imaging and reconstruction of post-implantation mouse development at the single-cell level. *Cell* **175**, 859–876. e833 (2018).
27. Royer, L. A. *et al.* Adaptive light-sheet microscopy for long-term, high-resolution imaging in living organisms. *Nat. Biotechnol.* **34**, 1267–1278 (2016).
28. Furlong, E. E. M. & Levine, M. Developmental enhancers and chromosome topology. *Science* **361**, 1341–1345 (2018).
29. Chen, H. *et al.* Dynamic interplay between enhancer-promoter topology and gene activity. *Nat. Genet.* **50**, 1296–1303 (2018).
30. Alexander, J. M. *et al.* Live-cell imaging reveals enhancer-dependent Sox2 transcription in the absence of enhancer proximity. *Elife* **8**, e41769 (2019).
31. Hnisz, D., Shrinivas, K., Young, R. A., Chakraborty, A. K. & Sharp, P. A. A phase separation model for transcriptional control. *Cell* **169**, 13–23 (2017).
32. Dooley, K. E., Warburton, A. & McBride, A. A. Tandemly integrated HPV16 can form a Brd4-dependent super-enhancer-like element that drives transcription of viral oncogenes. *mBio* **7**, e01446–16 (2016).
33. Crocker, J. C. & Grier, D. G. Methods of digital video microscopy for colloidal studies. *J. Colloid Interf. Sci.* **179**, 298–310 (1996).
34. Yildiz, A. *et al.* Myosin V walks hand-over-hand: Single fluorophore imaging with 1.5-nm localization. *Science* **300**, 2061–2065 (2003).
35. Pertsinidis, A., Zhang, Y. & Chu, S. Subnanometre single-molecule localization, registration and distance measurements. *Nature* **466**, 647–651 (2010).
36. Churchman, L. S. & Spudich, J. A. Colocalization of fluorescent probes: Accurate and precise registration with nanometer resolution. *Cold Spring Harb. Protoc.* **2012**, 141–149 (2012).
37. Pertsinidis, A. *et al.* Ultrahigh-resolution imaging reveals formation of neuronal SNARE/Munc18 complexes in situ. *Proc. Natl. Acad. Sci. USA* **110**, E2812–2820 (2013).
38. Wang, G., Hauver, J., Thomas, Z., Darst, S. A. & Pertsinidis, A. Single-molecule real-time 3d imaging of the transcription cycle by modulation interferometry. *Cell* **167**, 1839–1852. e1821 (2016).
39. Kepten, E., Bronshtein, I. & Garini, Y. Improved estimation of anomalous diffusion exponents in single-particle tracking experiments. *Phys. Rev. E Stat. Nonlin. Soft Matter Phys.* **87**, 052713 (2013).
40. Li, G. *et al.* Extensive promoter-centered chromatin interactions provide a topological basis for transcription regulation. *Cell* **148**, 84–98 (2012).
41. Zhou, X. *et al.* The human epigenome browser at Washington University. *Nat. Methods* **8**, 989–990 (2011).

Acknowledgements

We thank Pai-Tseng Kuo and Hsin-Wei Wen (MSKCC Structural Biology) for assistance in creating the dCas9-GFP U2 O-S cell line, Vidur Garg and Kat Hadjantonakis (MSKCC Developmental Biology) and Willie Mark (MSKCC Mouse Genetics Core Facility) for assistance with mouse embryo microinjection, Luciano Marraffini (Rockefeller University) for useful discussions and Luke Lavis (HHMI/Janelia) for dye-labeling reagents. This work was supported by the Louis V. Gerstner, Jr. Young Investigators Fund (A.P.), a National Cancer Institute grant (P30 CA008748), a National Institutes of Health (NIH) Director's New Innovator Award (1DP2GM105443-01; A.P.) and the National Institute of General Medical Sciences of NIH (1R01GM135545-01 and 1R21GM134342-01; A.P.).

Author contributions

Y.G. and A.P. designed and performed experiments. A.P. wrote the manuscript.

Competing interests

The authors declare no competing interests.

Additional information

Supplementary Information The online version contains supplementary material available at <https://doi.org/10.1038/s41598-021-91787-y>.

Correspondence and requests for materials should be addressed to A.P.

Reprints and permissions information is available at www.nature.com/reprints.

Publisher's note Springer Nature remains neutral with regard to jurisdictional claims in published maps and institutional affiliations.



Open Access This article is licensed under a Creative Commons Attribution 4.0 International License, which permits use, sharing, adaptation, distribution and reproduction in any medium or format, as long as you give appropriate credit to the original author(s) and the source, provide a link to the Creative Commons licence, and indicate if changes were made. The images or other third party material in this article are included in the article's Creative Commons licence, unless indicated otherwise in a credit line to the material. If material is not included in the article's Creative Commons licence and your intended use is not permitted by statutory regulation or exceeds the permitted use, you will need to obtain permission directly from the copyright holder. To view a copy of this licence, visit <http://creativecommons.org/licenses/by/4.0/>.

© The Author(s) 2021